ARTICLE

# Silanization of Ag-Deposited Magnetite Particles: An Efficient Route to Fabricate Magnetic Nanoparticle-Based Raman Barcode Materials

**Kwan Kim,*,† Jeong-Yong Choi,† Hyang Bong Lee,† and Kuan Soo Shin*,‡**

Department of Chemistry, Seoul National University, Seoul 151-742, Korea and Department of Chemistry, Soongsil University, Seoul 156-743, Korea

**ABSTRACT** Silica-coated Ag nanostructures usable as magnetic nanoparticle-based Raman barcode materials were developed. Initially, 283 nm sized spherical magnetite particles composed of 13 nm sized superparamagnetic $Fe_3O_4$ nanoparticles were synthesized, and silver deposition was conducted using butylamine as the reductant of $AgNO_3$ in ethanol. The Ag-deposited $Fe_3O_4$ ($Fe_3O_4$@Ag) particles are found to be efficient surface-enhanced Raman scattering (SERS) substrates with the enhancement factor at 632.8 nm excitation to be about $3 \times 10^6$. After SERS markers such as benzenethiol, 4-mercaptotoluene, 4-aminobenzenethiol, and 4-nitrobenzenethiol were adsorbed onto the silver surface, poly(allylamine hydrochloride) (PAH) was coated onto them using the layer-by-layer deposition method such that a subsequent base-catalyzed silanization could readily form a 60 nm thick silica shell around the PAH layer by a biomimetic process. The cross-linked silica shells effectively prevented the SERS-marker molecules from being liberated from the surface of the $Fe_3O_4$@Ag particles. Although the gram magnetization decreased nearly to one-half of the initial value because of coating with silver and silica, the remaining magnetization was nonetheless strong enough for the silica-coated $Fe_3O_4$@Ag particles to be used as barcode materials operating via SERS.

**KEYWORDS:** $Fe_3O_4$ particle • silver deposition • silanization • surface-enhanced Raman scattering • nanoparticle-based barcode material

## 1. INTRODUCTION

Magnetic nanoparticles are a class of nanoparticle that can be manipulated using magnetic fields (1, 2). Such particles commonly consist of magnetic elements such as iron, nickel, and cobalt and their chemical compounds (3, 4). These particles have been the focus of much research recently because they possess attractive properties that could see potential use in catalysis, biomedicine, magnetic resonance imaging, data storage, and environmental remediation (5−8). Nonmagnetic metal nanoparticles have also attracted a great deal of interest today (9−13). Among others, gold and silver nanoparticles are receiving great attention because of their unique optical properties associated with surface plasmon resonance (14−18). Because of the latter characteristics, Ag and Au nanostructures exhibit surface-enhanced Raman scattering (SERS) phenomena that can be used as a means for analyzing organic adsorbates at submonolayer coverages: SERS is a phenomenon in which the scattering cross-sections of molecules adsorbed onto gold and silver surfaces are dramatically enhanced. In general, two enhancement mechanisms—one referred to as a long-range electromagnetic (EM) effect and the other a short-range chemical effect—are believed to be simultaneously operational in SERS (19, 20). Ag- or Au-deposited magnetic particles would then be useful especially in the Raman spectroscopic analysis of chemical species dissolved in aqueous solutions because the magnetic particles could readily be recovered from the solution phase using a magnet without centrifugation and/or filtering (21−25).

We recently demonstrated that Ag-deposited $Fe_2O_3$ nanoparticles are efficient SERS substrates for the vibrational spectroscopic characterization of molecular adsorbates prepared in a similar way on silver surfaces (5, 25). The $Fe_2O_3$ (hematite) particles used earlier were commercial products with very irregular shape and size distribution. Accordingly, it was difficult to enjoy fully the properties of superparamagnetism of nanometer sized magnetite particles. In this work, we have first synthesized spherical $Fe_3O_4$ (magnetite) particles with a mean diameter of 283 nm, but are actually composed of ~13 nm superparamagnetic particles onto which Ag nanoaggregates are finally assembled to endow them with both the superparamagnetism and SERS activity. Ag-deposited magnetic nanoparticles would then be used as a core material of molecular sensors and barcodes both of which are operating via SERS. One difficulty in the latter application is the necessity for the stabilization of SERS marker molecules adsorbed on Ag nanoaggregates. It is well-

* To whom all correspondence should be addressed. E-mail: kwankim@snu.ac.kr (K.K.); kshin@ssu.ac.kr (K.S.S.). Tel: +82-2-8806651 (K.K.); +82-2-8200436 (K.S.S.). Fax: +82-2-8891568 (K.K.); +82-2-8244383 (K.S.S.).
Received for review March 12, 2010 and accepted June 17, 2010
† Seoul National University.
‡ Soongsil University.
DOI: 10.1021/am1002074



Published on Web 06/29/2010

known that silica shells are biocompatible and stable (26−28). The fabrication of silica shells would then be an effective strategy to protect SERS marker molecules, and silica shells, once fabricated, can further be derivatized to possess biofunctional groups (29−34). Regarding silicification, however, a large amount of information has been gathered recently from bioinspired silica studies that have led to the development of silica films via soft matter routes (35−37). We demonstrated that once the SERS marker molecules are coated with aliphatic polyelectrolytes such as poly(allylamine hydrochloride), the base-catalyzed silanization can be readily carried out to form stable silica shells around the polyelectrolyte layers by a biomimetic process (29).

In this work, we have succeeded in coating Ag-deposited magnetite particles smoothly with silica overlayers, without affecting the SERS spectral features of various marker molecules assembled on the Ag nanoaggregates. At first, superparamagnetic magnetite particles with a mean diameter of ∼300 nm were prepared, and then SERS-active Ag nanoaggregates were fabricated onto them by a very simple electroless-deposition method. This method requires only the incubation of magnetite particles in a solution of silver ions with butylamine at moderate temperatures. SERS-active Ag nanostructures are then formed exclusively on magnetite particles by the reduction activity of butylamine. Because butylamine is a very mild reductant, bulk reaction does not take place. Various aromatic thiol molecules were subsequently adsorbed, as SERS markers, onto the Ag nanoaggregates by a self-assembly method. In the final stage, a biomimetic base-catalyzed silanization was carried out to form stable silica shells around the SERS markers following the layer-by-layer deposition of cationic and anionic aliphatic polyelectrolytes onto them. The method is cost-effective and is suitable for mass production, so that the silica coated SERS-active magnetic particles can be expected to find application in a variety of fields including smart barcodes for product tracking, document protection, and multiplexing of biological molecules (38, 39). In particular, the widespread dissemination of counterfeit products and documents has led to growing demands for efficient analytical tools for identifying those items. In addition, major health and security concerns have generated urgent needs for screening multiple analytes in a single assay. Encoded nanomaterials, with a large number of readily distinguishable barcode patterns, are therefore particularly attractive for meeting the requirements of product tracking and multiplexed biodetection.

## 2. EXPERIMENTAL PROCEDURES

**Chemicals.** Ferric chloride six hydrate ($FeCl_3 \cdot 6H_2O$), silver nitrate ($AgNO_3$), sodium acetate, tetraethyl orthosilicate (TEOS, 98%), butylamine (99%), benzenethiol (BT, 99+%), 4-aminobenzenethiol (4-ABT, 97%), 4-nitrobenzenethiol (4-NBT, 80%), 4-mercaptotoluene (4-MT, 98%), rhodamine B isothiocyanate (RhBITC, 97%), polyethylene glycol (MW ∼3400 Da), poly(allylamine hydrochloride) (PAH, MW 70 kDa), poly(acrylic acid) (PAA, MW 100 kDa)), and silver powder ($\mu$Ag, 99.9+%) with a particle size of 2.0−3.5 $\mu$m were purchased from Aldrich and used as received. Ammonia solution (28−30 wt %) was obtained from Sanchun Pure Chemical Company. Other chemicals, unless specified, were of reagent grade, and highly purified water, of resistivity greater than 18.0 MΩ cm, was used throughout the experiments.

**Synthesis of $Fe_3O_4$ Particles.** Spherically shaped $Fe_3O_4$ particles were synthesized following the protocols of Deng et al. (40). Initially, $FeCl_3 \cdot 6H_2O$ (1.35 g, 5 mmol) was dissolved in ethylene glycol (40 mL) to form a clear solution, followed by the addition of sodium acetate (3.6 g) and polyethylene glycol (1.0 g). The mixture was stirred vigorously for 30 min and then refluxed at 200 °C for 24 h. After being cooled to room temperature, the black products were washed several times with ethanol and then dried at 60 °C for 6 h. The formation of $Fe_3O_4$ was confirmed by X-ray diffraction (XRD). According to transmission electron microscopy (TEM) images, the size of $Fe_3O_4$ particles was approximated to be ∼283 nm in diameter.

**Preparation of Ag-Deposited $Fe_3O_4$ ($Fe_3O_4$@Ag) Particles.** To deposit silver onto the magnetite particles, we placed the cleaned 1 mg $Fe_3O_4$ powder in a polypropylene container into which 10 mL of an ethanolic silvering solution was added and then incubated it for 50 min at 50 °C with vigorous shaking. As a silvering mixture, the concentration of $AgNO_3$ was maintained at 4 mM, whereas that of butylamine was subject to change from 0.4 to 4 mM. The polypropylene container was used to avoid nonspecific silvering of the reaction vessel. After being rinsed with ethanol, the Ag-deposited $Fe_3O_4$ ($Fe_3O_4$@Ag) particles were redispersed in ethanol under sonication for 5 min.

**Derivatization of $Fe_3O_4$@Ag with Raman Markers ($Fe_3O_4$@Ag/Raman).** In order to use $Fe_3O_4$@Ag particles as a core material for nanoparticle-based barcode operating via SERS, aromatic thiol molecules such as BT, 4-MT, 4-ABT, and 4-NBT were assembled as a Raman marker onto the $Fe_3O_4$@Ag particles and then three bilayers of PAA and PAH were deposited onto the $Fe_3O_4$@Ag/Raman particles as a spacer layer before silanization. Specifically, 20 mg of $Fe_3O_4$@Ag particles was placed first in a vial into which 10 mL of 1 mM ethanolic BT (or 4-MT, 4-ABT, 4-NBT) solution was added. After 3 h, the $Fe_3O_4$@Ag/Raman particles were separated from the mixture by using a neodium magnet and then rinsed with ethanol to remove the excess Raman markers. Polyelectrolyte layers were formed by the sequential dipping of the $Fe_3O_4$@Ag/Raman particles into the PAA and PAH solutions (2 mg $mL^{-1}$) for 10 min at room temperature; the pH of the PAH solution was 5.0, while that of PAA solution was 4.2. In the interim, to change the polyelectrolyte solution, magnetite particles were intensively rinsed with water. In the final state, the outermost layer, PAH, was subjected to silanization as described below.

**Further Silanization of $Fe_3O_4$@Ag/Raman Particles.** Silanization was performed using a method similar to that described by Xia and co-workers (41). Initially, 20 mg of PAH-capped $Fe_3O_4$@Ag/Raman particles was weighed and then poured, under sonication, into a mixture composed of 5 mL of water and 35 mL of ethanol. To this mixture were added 0.5 mL of ammonia (9.4 M) and 0.5 mL of TEOS (4.4 M), and the whole mixture was then left to react for 2 h at room temperature. The reacted particles were collected using a permanent magnet, and rinsed with water and ethanol.

**Instrumentation.** UV−vis spectra were obtained with a SINCO S-4100 UV−vis absorption spectrometer. The magnetic properties were measured using a Quantum Design SQUID Magnetometer. TEM images were obtained on a LIBRA-120 transmission electron microscope at 120 kV. XRD patterns were obtained on a MAC Science Co M18XHF-SRA powder diffractometer for a $2\theta$ range of 30−80° at an angular resolution of 0.05° using Cu K$\alpha$ (1.5406 Å) radiation. Zeta potential measurements were carried out on a Zetasizer 3000HS (Malvern Instruments, U.K.), using Zetasizer 3000 Advanced Zeta Mode v1.61 software for data acquisition. Infrared spectra were obtained using a Bruker IFS 113v FT-IR spectrometer equipped

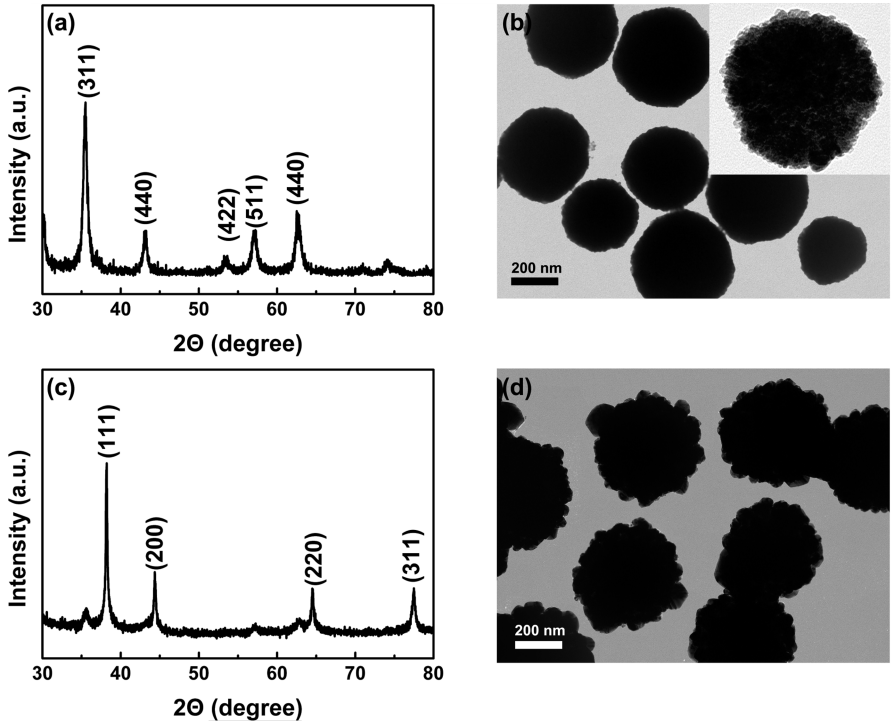


**FIGURE 1. (a) XRD pattern and (b) TEM image of $Fe_3O_4$ particles synthesized in this work. (c) XRD pattern and (d) TEM image of $Fe_3O_4$@Ag particles prepared in a 1:1 mixture of $AgNO_3$ and butylamine.**

with a Globar light source and a liquid-$N_2$-cooled wide-band mercury cadmium telluride detector. Raman spectra were obtained using a Renishaw Raman system model 2000 spectrometer. Either the 514.5 nm line from a 20 mW $Ar^+$ laser (Melles-Griot model 351MA520) or the 632.8 nm line from a 17 mW He/Ne laser (Spectra Physics model 127) was used as the excitation source. Raman scattering was detected over 180° with a Peltier cooled (−70 °C) charge-coupled device (CCD) camera (400 × 600 pixels). The data acquisition time was usually 30 s, and the measured intensity was normalized with respect to that of a silicon wafer at 520 $cm^{-1}$.

## 3. RESULTS AND DISCUSSION

**Characterization of $Fe_3O_4$@Ag Particles.** All the XRD peaks of iron oxides synthesized in this work could be indexed to the magnetite structure of $Fe_3O_4$ (JCPDS 75−1609), as in Figure 1a. The average size of the $Fe_3O_4$ nanoparticles deduced from Sherrer's formula is about 13 nm. According to the TEM image (see Figure 1b), $Fe_3O_4$ particles were spherical, but with a mean diameter of 283 ± 39 nm. The discrepancy between the XRD and TEM data could be understood by assuming that the 283 nm sized particles were actually composed of 13 nm sized $Fe_3O_4$ nanoparticles. This suggests that $Fe_3O_4$ nanoparticles have self-assembled into spherical aggregates. In fact, a close look at the TEM image (inset of Figure 1b) indicated that the large particles consisted of agglomeration of smaller particles. Disordered pores existed among the primary nanoparticles but within spherical aggregates.

Figure 2a shows the magnetization curve of $Fe_3O_4$ particles measured at room temperature. The curve presents a small hysteresis loop, and the magnetic saturation value is ~78 emu/g. From a magnified view of the magnetization curve at low applied fields, the remnant $M_r$ defined as the

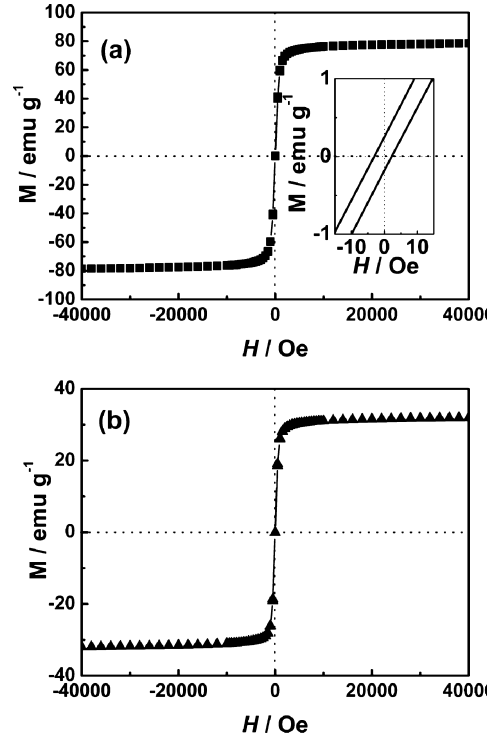


**FIGURE 2. (a) Magnetization curve of the as-prepared $Fe_3O_4$ particles measured at room temperature: inset shows a magnified view at low applied fields. (b) Similar magnetization curve measured for silanized $Fe_3O_4$@Ag particles.**

magnetization at $H = 0$ is about 0.22 emu/g, whereas the coercity $H_c$ defined as the field magnitude necessary to obtain $M = 0$ is about 2.5 Oe. It has been reported that the magnetic $Fe_3O_4$ particles exhibit superparamagnetic behavior when the particle size decreases to below a critical value, generally around 20 nm. The relatively high $M_s$ value with

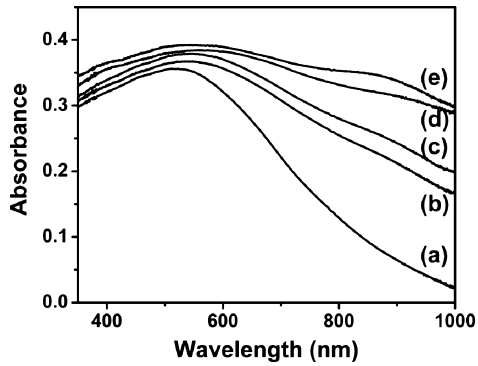


FIGURE 3. UV−vis spectra of $Fe_3O_4$ particles dispersed in ethanol taken (a) before and (b−e) after silvering onto them at molar ratios of (b) 1:0.1, (c) 1:0.25, (d) 1:0.5, and (e) 1:1 of $AgNO_3$ and butylamine. The concentration of $AgNO_3$ was maintained at 4 mM in all silvering processes.

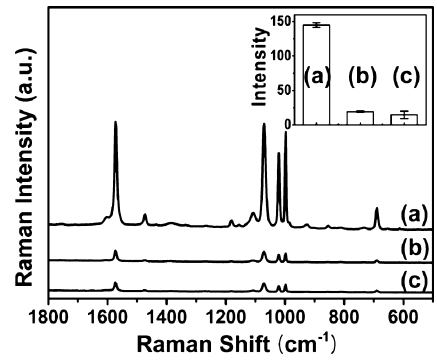


FIGURE 4. SERS spectra of BT adsorbed on $Fe_3O_4$@Ag particles that have been prepared from solutions of $AgNO_3$:butylamine ratios of (a) 1:1 and (b) 1:0.1. (c) SERS spectrum of BT adsorbed on $\mu$Ag powders taken for comparison. Inset: SERS intensity of the ring breathing band of BT at 1573 $cm^{-1}$ versus the samples corresponding to a−c.

relatively low $H_c$ and $M_r$ values in this work can then be attributed to the small primary particle size of about 13 nm in dimension, as well as to the oriented attachment of primary particles in large spherical aggregates.

A zeta potential measurement indicates that $Fe_3O_4$ particles are negatively charged in absolute ethanol, i.e., −16.3 ± 1.6 mV, suggesting that their surface sites are occupied by oxygen atoms rather than iron atoms. As silver ions are added into the solution, the negative charges are gradually neutralized, suggesting that oxygen atoms are bound by $Ag^+$ ions. In the presence of butylamine, the surface-bound $Ag^+$ ions are reduced and the silver particles thus formed subsequently function as seeds for the growth of Ag shells on $Fe_3O_4$ particles. In the actual deposition of silver onto $Fe_3O_4$, the concentration of $AgNO_3$ was maintained at 4 mM, while that of butylamine was subject to change. When very dilute butylamine was used, Ag nanoparticles with sizes of 5−20 nm formed over the $Fe_3O_4$ surfaces, but increasing the concentration of butylamine resulted in much larger Ag nanoparticles being formed. Figure 1d shows the TEM image taken after the deposition of silver at 1:1 molar ratio of $AgNO_3$ and butylamine. The deposition of silver onto $Fe_3O_4$ can be confirmed from the corresponding XRD data shown in Figure 1c. The four peaks appearing at $2\theta$ values of 38.1, 44.3, 64.4, and 77.3° can be attributed to the reflections of the (111), (200), (220), and (311) crystalline planes of cubic Ag, respectively (42). According to the Debye−Scherrer equation, the size of the Ag nanoparticles is estimated to be ~24 nm (43).

Figure 3b−e show the UV−vis spectra of $Fe_3O_4$@Ag particles prepared at molar ratios of 1:0.1, 1:0.25, 1:0.5, and 1:1 of $AgNO_3$ and butylamine, respectively. For reference, the UV−vis spectrum of unmodified $Fe_3O_4$ particles is shown in Figure 3a. We have to mention that prior to taking the UV−vis spectra, the $Fe_3O_4$@Ag particles were isolated from the reaction mixture using a magnet and redispersed into fresh ethanol, and then subjected to gentle sonication. The UV−vis spectra of the remaining reaction mixtures were featureless, indicating that silver nanoparticles were not formed, at least not in the bulk solution. The reduction of silver must have occurred only on the surfaces of $Fe_3O_4$ particles. Butylamine is a very weak reductant, so it seemed that nucleation centers hardly ever form in the solution. However, once silver ions are bound to the oxygen sites of the $Fe_3O_4$ particles as described previously, silver nitrate will be reduced by butylamine, anchoring onto modified $Fe_3O_4$ surfaces.

It is seen from Figure 3 that the UV−vis spectral feature of $Fe_3O_4$ changes as it is treated with the silvering medium. Upon the deposition of silver, not only the absorbance at shorter wavelengths but also the absorbance at longer wavelengths is noticeably increased. The absorbance increase around 400 nm is presumed to be due to a Mie plasmon resonance excitation from the silver nanoparticles. Evidently, the surface plasmon absorption (SPA) band of Ag deposited on $Fe_3O_4$ surface broadened as the amount of butylamine increased. We believe that the plasmon coupling between the deposited Ag nanoparticles, as well as the interface structure between the Ag and $Fe_3O_4$ of the hybrid particles, may play a crucial role for the red shift and broadening of the SPA band. Consulting the electromagnetic mechanism of SERS, those $Fe_3O_4$@Ag particles must be efficient SERS substrates under the irradiation of a visible laser. We thus evaluated their performance as SERS substrates, using BT as the model SERS marker.

**SERS of $Fe_3O_4$@Ag/Raman Particles.** Spectra a and b in Figure 4 show the two typical SERS spectra of BT adsorbed on $Fe_3O_4$@Ag particles that have been prepared from solutions of $AgNO_3$:butylamine ratios of 1:1 and 1:0.1, respectively. As expected from the UV−vis spectra, the SERS peaks in Figure 4a are very intense while the peaks in Figure 4b are comparatively weak. This clearly reflects the different optical absorption characteristics of the two samples. For reference, Figure 4c shows the SERS spectrum of BT adsorbed on $\mu$Ag powders, which are effective substrates for the IR and Raman spectroscopic characterization of molecular adsorbates (44, 45). The reason for taking the latter spectrum was first simply to compare its SERS activity with that of $Fe_3O_4$@Ag particles, but it was intended, if possible, to figure out the enhancement factor (EF) of $Fe_3O_4$@Ag particles indirectly by comparing their SERS activities under the same experimental conditions. It is seen that the SERS peaks in Figure 4a are an order of magnitude stronger than

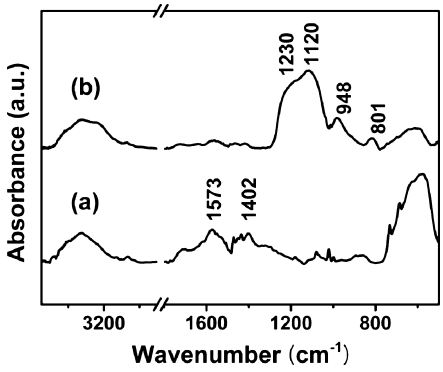


**FIGURE 5. (a) Diffuse reflectance infrared spectrum taken after three bilayers of PAA/PAH were deposited onto the BT adsorbed $Fe_3O_4$@Ag particles and (b) that taken further after silanization onto the PAA/PAH layer.**

the corresponding ones in Figure 4c. Recalling the fact that the EF of BT (with 632.8 nm excitation) adsorbed on $\mu$Ag powders was determined to be $3.8 \times 10^5$ (46), the EF factor of BT on $Fe_3O_4$@Ag particles should well be more than $3 \times 10^6$. Another noteworthy point is that the SERS peak of BT at 632.8 nm excitation shown in Figure 4 is more intense than that at 514.5 nm excitation (data not shown). This may be attributed to greater electromagnetic enhancement due to the larger absorbance of $Fe_3O_4$@Ag particles at 632.8 nm than at 514.5 nm with respect to that of neat $Fe_3O_4$, as can be seen in UV−vis spectra a and e in Figure 3.

**Silica-Coated $Fe_3O_4$@Ag/Raman Particles.** Subsequently, the silanization reaction is carried out to protect the SERS markers assembled onto $Fe_3O_4$@Ag particles. The silica coating cannot be performed directly onto the SERS markers, however. When it was possible, the SERS spectral feature of the marker molecules was degraded too much by their direct contact with the siloxane groups. We found recently that once the SERS marker molecules are coated with aliphatic polyelectrolytes such as PAH, the base-catalyzed silanization can be readily carried out to form stable silica shells around the polyelectrolyte layers by a biomimetic process. The SERS spectral feature of the marker molecules is not deteriorated in this case. Hence, three bilayers of PAA and PAH were deposited, before silanization, onto the $Fe_3O_4$@Ag particles following the adsorption of marker molecules. The successful deposition of PAA and PAH polyelectrolytes was confirmed from the growth of the $COO^-$ stretching bands in the IR spectrum: the bands around 1402 and 1573 $cm^{-1}$ in Figure 5a are due to the symmetric and antisymmetric stretching vibrations of the carboxylate groups of PAA, respectively (47, 48). The successful silanization can also be confirmed from the IR spectrum shown in Figure 5b. The two strong bands appearing at ~1230 and ~1120 $cm^{-1}$, as well as a somewhat weaker band at ~801 $cm^{-1}$, can be attributed to the vibrational modes involving the bridging oxygen atoms in Si−O−Si moieties, whereas the peak at ~948 $cm^{-1}$ is due to the Si−O stretching vibration of the Si−OH bonds (49, 50). The formation of silica shells must have proceeded by adsorption of nuclei and small particles from solution onto the $Fe_3O_4$@Ag particles due to the electrostatic attraction between the positively

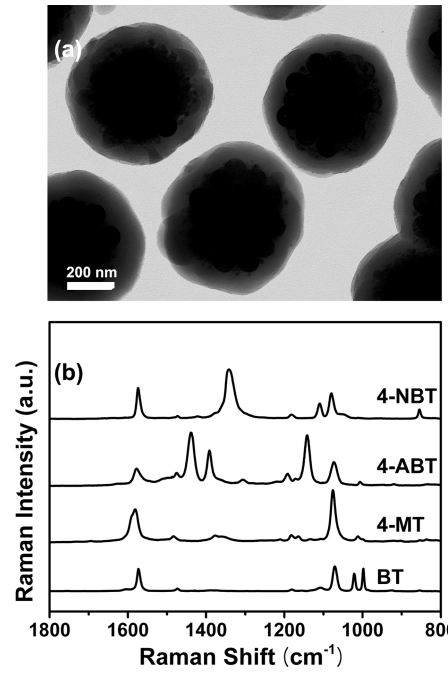


**FIGURE 6. (a) TEM image of silica-coated $Fe_3O_4$@Ag particles. (b) Raman spectra of silica-coated $Fe_3O_4$@Ag particles containing BT, 4-MT, 4-ABT, and 4-NBT as SERS markers (from bottom to top) taken after soaking them in 0.1 mM ethanolic RhBITC solution for 24 h.**

charged amine groups of PAH and the anionic silica species, followed by particle growth.

According to the TEM image (see Figure 6a), the silica shell thickness is estimated to be about 58 nm. From the TEM image alone, it is not evident, however, whether or not the $Fe_3O_4$@Ag particles are covered fully with silica shells without any defect. We thus conducted a place exchange reaction to occur on $Fe_3O_4$@Ag particles with RhBITC. RhBITC is a very strong Raman scatterer and is also known to adsorb to such an extent on Ag that BT on Ag, for instance, can be exchanged with RhBITC. The RhBITC peaks are identified immediately when $Fe_3O_4$@Ag/BT particles are soaked in the dye. However, we do not observe any RhBITC peak when silanized $Fe_3O_4$@Ag/BT particles are subjected to the place exchange reaction with RhBITC for 24 h. A similar experiment is repeated with samples containing 4-MT, 4-ABT, and 4-NBT as SERS markers. As shown in Figure 6b, the observed spectra all are due to SERS-marker molecules used initially to modify $Fe_3O_4$@Ag particles. These Raman spectral data clearly illustrate that all $Fe_3O_4$@Ag particles are fully coated with silica shells without any defect.

The exclusive appearance of the Raman peaks due to BT, 4-MT, 4-ABT, and 4-NBT in Figure 6b is not surprising because aliphatic polyelectrolytes such as PAA and PAH and inorganic materials such as silica are weak Raman scatterers, and the SERS signal must be derived mostly from the adsorbate that is in direct contact with the SERS substrates in accordance with electromagnetic and chemical enhancement mechanisms. To use silica-coated $Fe_3O_4$@Ag particles as barcode materials, these SERS peaks have to be maintained for an extended time period. In this regard, we have examined the extent to which the SERS spectra are subjected to change when silica-coated $Fe_3O_4$@Ag particles are left in

an ambient condition or soaked in Millipore water, ethanol, or phosphate-buffered saline (PBS) solution for up to 30 days. In all cases, the SERS spectral features were invariant (data not shown). We also confirmed that once silica-coated $Fe_3O_4$@Ag particles are spin-coated on bulk magnetic discs, they remain intact even in wet environments. This must be due to the superparamagnetic property of $Fe_3O_4$ particles. As shown in Figure 2b, the magnetic saturation value per gram obviously decreases to one-half of the initial value after coating with silver and silica. The decrease in the magnetization is due to the additional masses of silver and silica deposited onto $Fe_3O_4$, coupled with their diamagnetic shielding. In any case, the apparent magnetic moment is strong enough for the silica-coated $Fe_3O_4$@Ag particles to be used as nanoparticle-based barcode materials operating via SERS. The particles were able to be magnetically concentrated and picked up readily using a small magnet.

## 4. CONCLUSIONS

First of all, we have successfully synthesized spherically shaped magnetite particles. According to the XRD and magnetization data, the 283 nm sized spherical particles were composed of 13 nm sized superparamagnetic $Fe_3O_4$ nanoparticles. To endow them with SERS activity, we conducted silver deposition using butylamine as a reducing agent of $AgNO_3$ in ethanol. The most SERS-active particles were manufactured in a 1:1 solution of $AgNO_3$ and butylamine. Comparing the SERS peaks of BT on $Fe_3O_4$@Ag and commercial $\mu$Ag powders, the EF factor of $Fe_3O_4$@Ag particles was estimated to be more than $3 \times 10^6$ (with 632.8 nm excitation). After Raman markers (BT or 4-MT, 4-ABT, 4-NBT) were adsorbed on Ag, three bilayers of PAA and PAH were deposited onto them by the layer-by-layer (LbL) deposition method, and then enclosed further by a silica shell ~60 nm in thickness. The latter silanization was readily accomplished at room temperature as in living systems due to the facile LbL deposition of polyelectrolytes irrespective of the kind of SERS markers. Thereby, the cross-linked silica shells prevented the SERS-marker molecules from being liberated from the surface of the $Fe_3O_4$@Ag particles for an extended time period in air or soaked in water, ethanol, and PBS solution. Upon coating with silver and silica, the gram magnetization has, however, decreased nearly to one-half of the initial value, but the remained magnetization was still strong enough for the silica-coated $Fe_3O_4$@Ag particles to be used as nanoparticle-based barcode materials operating via SERS.

**Acknowledgment.** This work was supported by National Research Foundation of Korea Grant funded by the Korean Government (Grants 2010-0001637, M10703001067-08M0300-06711-Nano2007-02943, KRF-2008-313-C00390, and 2009-0072467).

### REFERENCES AND NOTES

(1) Xu, C.; Sun, S. *Polym. Int.* **2007**, *56*, 821–826.
(2) Leem, G.; Sarangi, S.; Zhang, S.; Rusakova, I.; Brazdeikis, A.; Litvinov, D.; Lee, T. R. *Cryst. Growth Des.* **2009**, *9*, 32–34.
(3) Davis, J. R. *Nickel, Cobalt, and Their Alloys*; ASM International: Materials Park, OH, 2000.
(4) Chen, D.-H.; Hsieh, C. -H. *J. Mater. Chem* **2002**, *12*, 2412–2415.
(5) Shin, K. S.; Choi, J. -Y.; Park, C. S.; Jang, H. J.; Kim, K. *Catal. Lett.* **2009**, *133*, 1–7.
(6) Pankhurst, Q. A.; Connolly, J.; Jones, S. K.; Dobson, J. *J. Phys. D: Appl. Phys.* **2003**, *36*, R167–R181.
(7) Lens, P. N.L.; Hemminga, M. A. *Biodegradation* **1998**, *9*, 393–409.
(8) Koch, C. C. *Nanostructured Materials; Processing, Properties, and Applications*: William Andrew Publishing: Norwich, NY, 2006.
(9) Barnes, W. L.; Dereux, A.; Ebbesen, T. W. *Nature* **2003**, *424*, 824–830.
(10) Bohren, C. F.; Huffman, D. R. *Absorption and Scattering of Light By Small Particles*; Wiley: New York, 1998.
(11) Gray, S. K.; Kupka, T. *Phys. Rev. B* **2003**, *68*, 045415/1−045415/11.
(12) Oliva, J. M.; Gray, S. K. *Chem. Phys. Lett.* **2003**, *379*, 325–331.
(13) Maier, S. A.; Kik, P. G.; Atwater, H. A.; Meltzer, S.; Harel, E.; Kowel, B. E.; Requicha, A. A. G. *Nat. Mater.* **2003**, *2*, 229–232.
(14) Haes, A. J.; Van Duyne, R. P. *J. Am. Chem. Soc.* **2002**, *124*, 10596–10604.
(15) Eustis, S.; El-Sayed, M. A. *Chem. Soc. Rev.* **2006**, *35*, 209–217.
(16) Jensen, T. R.; Malinsky, M. D.; Haynes, C. L.; Van Duyne, R. P. *J. Phys. Chem. B* **2000**, *104*, 10549–10556.
(17) Haes, A. J.; Zou, S.; Schatz, G. C.; Van Duyne, R. P. *J. Phys. Chem. B.* **2004**, *108*, 6961–6968.
(18) Malinsky, M. D.; Kelly, K. L.; Schatz, G. C.; Van Duyne, R. P. *J. Am. Chem. Soc.* **2001**, *123*, 1471–1482.
(19) Chang, R. K.; Furtak, T. E., Eds. *Surface Enhanced Raman Scattering*; Plenum Press: New York, 1982.
(20) Moskovits, M. *Rev. Mod. Phys.* **1985**, *57*, 783–826.
(21) Lyon, J. L.; Fleming, D. A.; Stone, M. B.; Schiffer, P.; Williams, M. E. *Nano Lett.* **2004**, *4*, 719–723.
(22) Cui, Y. L.; Hu, D. D.; Fang, Y. *Sci. China, Ser. B: Chem.* **2001**, *44*, 404–410.
(23) Yu, A.; Geng, T.; Fu, Q.; Chen, C.; Cui, Y. *J. Magn. Magn. Mater.* **2007**, *311*, 421–424.
(24) Haruta, M.; Yamada, N.; Kobayashi, T.; Iijima, S. *J. Catal.* **1989**, *15*, 301–309.
(25) Kim, K.; Jang, H. J.; Shin, K. S. *Analyst* **2009**, *134*, 308–313.
(26) Barbé, C.; Bartlett, J.; Kong, L.; Finnie, K.; Lin, H. Q.; Larkin, M.; Calleja, S.; Bush, A.; Calleja, G. *Adv. Mater.* **2004**, *16*, 1959–1966.
(27) Harrell, T. M.; Hosticka, B.; Power, M. E.; Cemke, L.; Hull, R.; Norris, P. M. *J. Sol−Gel Sci. Technol.* **2004**, *31*, 349–352.
(28) Kros, A.; Gerritsen, M.; Sprakel, V. S. I.; Sommerdijk, N. A. J. M.; Jansen, J. A.; Nolte, R. J. M. *Sens. Actuators, B* **2001**, *81*, 68–75.
(29) Kim, K.; Lee, H. B.; Shin, K. S. *Langmuir* **2008**, *24*, 5893–5898.
(30) Green, M.; Harries, J.; Wakefield, G.; Taylor, R. *J. Am. Chem. Soc.* **2005**, *127*, 12812–12813.
(31) Philipse, A. P.; van Bruggen, M. P. B.; Pathmamanoharan, C. *Langmuir* **1994**, *10*, 92–99.
(32) Spuch-Calvar, M.; Rodríguez-Lorenzo, L.; Morales, M. P.; Álvarez-Puebla, R. A.; Liz-Marzán, L. M. *J. Phys. Chem. C.* **2009**, *113*, 3373–3377.
(33) Fernández-López, C.; Mateo-Mateo, C.; Álvarez-Puebla, R. A.; Pérez-Juste, J.; Pastoriza-Santos, I.; Liz-Marzán, L. M. *Langmuir* **2009**, *25*, 13894–13899.
(34) Sanles-Sobrido, M.; Exner, W.; Rodríguez-Lorenzo, L.; Rodríguez-González, B.; Correa-Duarte, M. A.; Álvarez-Puebla, R. A.; Liz-Marzán, L. M. *J. Am. Chem. Soc.* **2009**, *131*, 2699–2705.
(35) Patwardhan, S. V.; Mukherjee, N.; Steinitz-Kannan, M.; Clarson, S. J. *Chem. Commun.* **2003**, 1122–1123.
(36) Coffman, E. A.; Melechko, A. V.; Allison, D. P.; Simpson, M. L.; Doktycz, M. J. *Langmuir* **2004**, *20*, 8431–8436.
(37) Sun, Q.; Vrieling, E. G.; Santen, R. A. V.; Sommerdijk, N. A.J.M *Curr. Opin. Solid State Mater. Sci.* **2004**, *8*, 111–120.
(38) Wang, J. *J. Mater. Chem.* **2008**, *18*, 4017–4020.
(39) Pregibon, D. C.; Toner, M.; Doyle, P. S. *Science* **2007**, *315*, 1393–1396.
(40) Deng, H.; Li, X.; Peng, Q.; Wang, X.; Chen, J.; Li, Y. *Angew. Chem., Int. Ed.* **2005**, *44*, 2782–2785.
(41) Xia, L.; Kim, N. H.; Kim, K. *J. Colloid Interface Sci.* **2007**, *306*, 50–55.
(42) He, R.; Qian, X.; Yin, J.; Zhu, Z. *J. Mater. Chem.* **2002**, *12*, 3783–3786.
(43) Birks, L. S.; Friedman, H. *J. Appl. Phys.* **1946**, *17*, 687–692.

(44) Han, S. W.; Han, H. S.; Kim, K. *Vib. Spectrosc.* **1999**, *21*, 133–142.
(45) Han, H. S.; Han, S. W.; Joo, S. W.; Kim, K. *Langmuir* **1999**, *15*, 6868–6874.
(46) Kim, K.; Lee, H. S.; Kim, N. H. *Anal. Bioanal. Chem.* **2007**, *388*, 81–88.
(47) Choi, J.; Rubner, M. F. *Macromolecules* **2005**, *38*, 116–124.
(48) Wang, Y.; Yu, A.; Caruso, F. *Angew. Chem., Int. Ed.* **2005**, *44*, 2888–2892.
(49) Tomozawa, M.; Hong, J.-W.; Ryu, S.-R. *J. Non-Cryst. Solids* **2005**, *351*, 1054–1060.
(50) Balamurugan, A.; Sockalingum, G.; Michel, J.; Fauré, J.; Banchet, V.; Wortham, L.; Bouthors, S.; Laurent-Maquin, D.; Balossier, G. *Mater. Lett.* **2006**, *60*, 3752–3757.

AM1002074